THERMOELECTRIC POWER GENERATION

IN DYNAMIC TEMPERATURE ENVIRONMENTS

by

Peter M. Attia

A thesis submitted to the Faculty of the University of Delaware in partial fulfillment of the requirements for the degree of Honors Degree in Chemical and Biomolecular Engineering with Distinction

Spring 2014

THERMOELECTRIC POWER GENERATION

IN DYNAMIC TEMPERATURE ENVIRONMENTS

by

Peter M. Attia

Approved: _____
Joshua M. O. Zide, Ph.D.
Professor in charge of thesis on behalf of the Advisory Committee

Approved: _____
Ajay K. Prasad, Ph.D.
Committee member from the Department of Mechanical Engineering

Approved: _____
Susan Groh, Ph.D.
Committee member from the Board of Senior Thesis Readers

Approved: _____
Michael Arnold, Ph.D.
Directory, University Honors Program

ACKNOWLEDGMENTS

First, I would like to thank Dr. Joshua Zide for taking a chance on an unproven freshman three years ago, giving me the initial opportunity to conduct research. I'm incredibly grateful for your endless patience and support, and my success is directly due to your investment in my education in research. I'm sure I would be hard pressed to find another undergraduate advisor who allows students to lead the direction of their research while always remaining available for feedback. I would also like to thank Pernell, Cory, Matt, Yujun, and the rest of the Zide group for encouragement and keeping things interesting in the lab.

Special thanks to the rest of my thesis committee: Dr. Ajay Prasad, for invaluable research feedback, paper edits, encouragement, and graduate school advice, and Dr. Susan Groh, for being the best freshman chemistry professor I could ask for. I know at least one graduating chemical engineer who would have lost his enthusiasm for the chemical field long ago if it weren't for your class. I'm proud to (hopefully!) join the three of you as Stanford alumni one day.

Much gratitude to Dr. Ismat Shah, in particular, for unforgettable travel experiences, mentorship, and hearty optimism. I'm blown away by your passion for sustainable engineering, cultural exchange, and peace, but I most admire your ability to form lasting friendships with people in Delaware, Marseilles, Islamabad, and, well, pretty much anywhere. I look to your example of a citizen-scientist as the ideal towards which I strive.

I would also like to attempt to thank other fantastic professors I have had at the University of Delaware, from whom I have learned so much: Dr. Thomas Powers, Dr. Bramie Lenhoff, Dr. Burnaby Munson, Dr. Prasad Dhurjati, Dr. Yushan Yan, and countless others. The Honors Program staff, particularly Kristin Bennighoff, Ray Peters, and Isabelle Lachat, were also incredibly helpful and patient with my Marshall and Gates-Cambridge scholarship applications; I consider my experience working with you a definite success, and I'm positive UD will have many scholarship winners soon.

My last and largest thanks goes to Mom, Dad, Ben, and Lucas for reasons that go without saying. I am so blessed to call you family.

TABLE OF CONTENTS

LIST OF TABLES

LIST OF FIGURES

ABSTRACT

Thermoelectric power generation from environments experiencing temporal temperature fluctuations is demonstrated; this source of power is useful for low-power devices in remote locations. In this thesis, devices that employ a thermoelectric module sandwiched between two heat exchangers with significantly different thermal masses are designed and characterized, and the effects of heat exchanger size and material selection, period of oscillation of the environmental temperature fluctuations, and radiative heat transfer on the thermoelectric power output are examined. Maximum experimental power generation on the order of milliwatts is reported using standard bismuth telluride thermoelectric modules in devices with a size of about 10 cm^3.

Chapter 1

INTRODUCTION

1.1   Motivation

Thermoelectric materials have long held promise as a critical piece of the sustainable-energy puzzle. The benefits of thermoelectric power are numerous: they capture energy from waste heat (such as that of industrial processes and automobile exhaust) and naturally-occurring thermal gradients (such as geothermal energy), have a small size, degrade slowly, generally consist of nontoxic materials, and operate silently. However, their widespread adaptation has been limited by their low power outputs and efficiencies. Although a large number of thermoelectric applications have been considered, investigated, and commercialized, the thermal driving force remains the same in each: a steady-state, spatial temperature gradient. In this thesis, an alternate source of thermal energy for thermoelectric power – transient thermal gradients, or the fluctuations of an environmental temperature with time – is investigated.

1.2   Background

Thermoelectric materials can generate a voltage from a spatial temperature gradient in a phenomenon termed the Seebeck effect. The generated voltage (ΔV) is proportional to the temperature gradient (ΔT), as given by Equation 1:

$$\Delta V = \alpha \Delta T \qquad (1)$$

Here, α is the proportionality constant, known as the Seebeck coefficient, between the voltage and the temperature gradient. For thermoelectric materials, the Seebeck coefficient is typically on the order of 10^{-4} V/K. Thermoelectric power generation (TPG) exploits thermal energy to generate electricity analogously to the use of light by PV solar cells, mechanical pressure by piezoelectric materials, and chemical potential energy by fuel cells.

From Equation 1, thermoelectric power generation is governed by Equation 2:

$$P = \frac{\Delta V^2}{R} = \frac{(\alpha \Delta T)^2}{R} \tag{2}$$

In Equation 2, R is the total resistance, or the sum of the external load resistance and the internal resistance of the thermoelectric. A TPG device consists of a thermoelectric module between two heat exchangers. In the simplest case, the heat exchangers are thin ceramic plates that physically support the thermoelectric elements and aid in heat distribution. The thermoelectric module consists of p-type and n-type thermoelectric elements alternating in series. Upon application of a heat source, the charge carriers (electrons and electron holes) diffuse through the material to lower the chemical potential gradient, thus decreasing the chemical potential gradient. The individual elements are connected by copper couples and supported by ceramic substrates. An illustration of a thermoelectric module, which is often termed a Peltier cooler for its application as a cooling device upon receiving an applied voltage, is given in Figure 1.
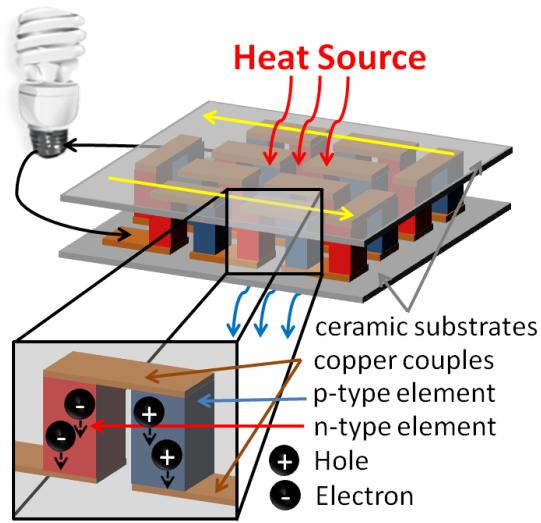
Figure 1:   Schematic of a thermoelectric module.

The power output of thermoelectric devices is significantly affected by heat exchanger and thermoelectric module geometries. Previously studied heat exchanger geometries include fins exposed to air [1] and spirals, zig-zags, and fins directing a liquid heat transfer medium [2]. Most thermoelectric modules are either bulk-based or thin films [3]; a unique variant of bulk-based modules are two-stage, or stacked, modules [4]. Optimization studies of bulk thermoelectric elements [5] and thin films [6] detail maximization of the power output of thermoelectric devices.

Thermoelectrics are typically characterized by the dimensionless "figure-of-merit", *ZT*, shown in Equation 3:

$$ZT = \frac{\sigma \alpha^2}{\kappa} T \qquad (3)$$

In Equation 3, σ is the electrical conductivity, α is the Seebeck coefficient, κ is the thermal conductivity, and *T* is the absolute temperature. Thermoelectric efficiency increases with increasing *ZT*; as *ZT* goes to infinity, the thermoelectric efficiency

approaches the Carnot efficiency [7]. Large ZT values are generally reported in nanoscale solid-state semiconductors; the highest reported ZT to date, found in a quantum-dot superlattice [8], is 3.5. Recently, high ZTs have been reported in semiconductors such as iron silicides [9], silicon nanowires [10], and nanoparticle-doped semiconductors [11–13]. Other materials, including polymers, have also been considered for thermoelectric applications, but their ZT values are typically very low (on order 10^{-3} to 10^{-2}) [14]. Bismuth telluride, Bi_2Te_3, remains the industry standard thermoelectric material for low-temperature (<400 K) TPG applications [15].

Among other applications, thermoelectrics are often deployed in environments containing a steady-state spatial temperature gradient as a means of waste-heat recovery [16]. Because thermoelectric conversion efficiencies are on the order of 5% [17], thermoelectric waste-heat recovery applications are most competitive when considerations of reliability and high energy losses override cost and efficiency; such applications include industrial steam condensers [18] and remote oil pipelines [19]. Additionally, thermoelectric tailpipes and radiators in automobiles exploit waste heat from hot exhaust gas [20] and engine coolant [21], respectively, to power internal car electronics. Thermoelectrics have also been considered for applications in remote locations using natural temperature gradients such as those powered by direct [22] or concentrated [23] solar radiation [24] and those found in the ocean [25].

While these steady-state thermoelectric applications are well established, other types of thermal gradients have not been thoroughly investigated. This proposal aims to explore thermoelectric power generation from transient, or time-varying, temperature environments, such as the diurnal variations of the day. This mechanism effectively requires the conversion of a *temporal* temperature gradient into a *spatial*

4

temperature gradient. This conversion is achieved by placing two heat exchangers with significantly different thermal inertias on either side of a thermoelectric plate. As the temperature of the environment changes with time, the temperature of each heat exchanger will respond at different rates, creating the spatial temperature difference required for power generation.

A comparison of steady-state and dynamic temperature gradients is illustrated by Figure 2.
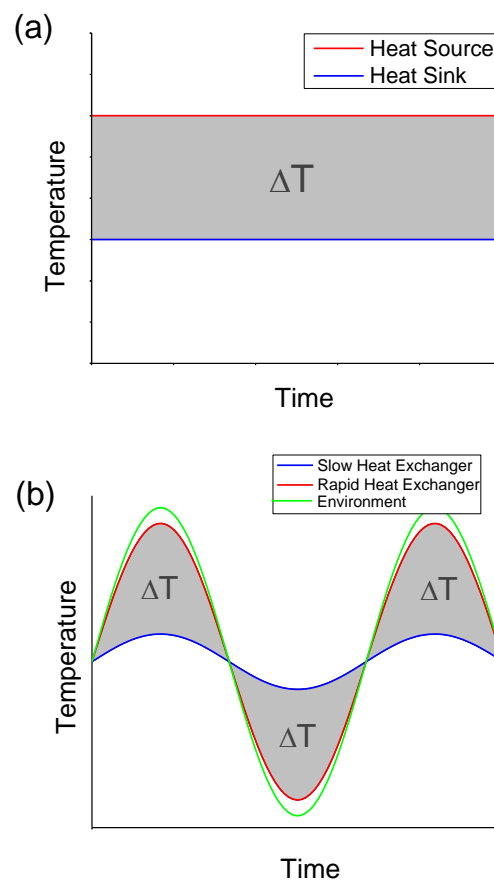
Figure 2:   Spatial (a) and temporal (b) thermal gradients.

Spatial temperature gradients, the conventional temperature gradient used for thermoelectric power, are constant with time (steady-state), and thus the thermoelectric power is constant with time. Temporal temperature gradients, the temperature gradient proposed for study, are not constant with time. A heat exchanger placed in this environment will respond to the environmental transient temperature gradient at a rate related to its material properties and its geometry; by placing two heat exchangers of different thermal response rates on either side of a thermoelectric, a spatial temperature gradient is created across the thermoelectric.

TPG based on temporal temperature gradients is not designed as a replacement for current centralized power distribution technology; rather, this mechanism of power generation is useful for small-scale power harvesting in remote environments where other power generation technologies are not practical.

Chapter 2

METHODOLOGY

2.1 Design Basis

To design efficient devices, the temperatures of the heat exchangers must be accurately known. A number of approximations have been developed for modeling the temperature dependence of an object in a convective environment; the appropriateness of a given model for a given object is governed by a dimensionless quantity known as the Biot number [26], defined in Equation 4:

$$\text{Bi} = \frac{hL}{\kappa} \qquad (4)$$

In this equation, h is the convective heat transfer coefficient and L is the characteristic length of the object (often defined as the ratio of volume to surface area) Small Biot numbers (<<1) indicate that heat transfer to the device is limited by boundary-layer convection, whereas large Biot numbers (>>1) indicate that the limiting mode of heat transfer is internal conduction. If the Biot number of an object is of order 1, a finite-element analysis, in which the object is subdivided into units assumed to be at a uniform temperature, is required to accurately predict the temperature within the object as a function of position and time; this analysis is computationally difficult, although commercial software packages exist. At extreme Biot numbers, some simplifying approximations can be made. The temperature of an object with a large Biot number can be modeled by the short-time penetration solution, in which the heat can be thought of as penetrating an infinite material; in contrast, the

temperature of an object with a small Biot number can be modeled with a lumped

parameter analysis, in which the entire object is assumed to be at a uniform

temperature. In this case, by rearranging Newton's law of convection, $\dot{Q} = hA(T_a -$

$T)$, and using a simple expression for the rate of temperature change of thermal mass,

$\dot{Q} = \rho V C_P dT/dt$, a relationship (Equation 5) is derived for the rate of temperature

change of the object, assuming the primary mode of heat transfer is convective:

$$\frac{dT}{dt} = \frac{h}{\rho C_p}\left(\frac{A}{V}\right)(T_a - T) = K(T_a - T) \tag{5}$$

In this equation, *dT/dt* is the temperature differential with respect to time, ρ is

the density, C_p is the specific heat capacity, *(A/V)* is the ratio of surface area to

volume, T_a is the ambient temperature, T is the object temperature, and K is a

proportionality constant termed the *thermal response rate coefficient*. If K is small, the

temperature of the object will remain uniform, regardless of the environmental

temperature; if K is large, the temperature of the object will change dramatically given

a small temperature difference between the object and its environment.

Thermoelectric power generation is proportional to the square of the

temperature difference across it; as a result, the temperatures of the heat exchangers on

either side of the thermoelectric plate should be as different as possible. This insight

on heat exchanger optimization suggests that the power output is proportional to the

ratio of thermal response rate coefficients of the two heat exchangers. Effectively, the

temperature of the rapid heat exchanger (small thermal mass; large K) approaches that

of the oscillating environmental temperature, while the temperature of the slow heat

exchanger (large thermal mass; small K) remains relatively constant with time. When

the *K/K* ratio is 1, both heat exchangers change temperature at the same rate, meaning

the temperature difference across the thermoelectric is zero, and no power is produced.

Clearly, to maximize the power output of these devices, the ratio of the heat exchanger thermal response rate coefficients should be maximized within the economic and size constraints of the application.

2.2 Theoretical Simulations

A numerical model was initially constructed in MATLAB to estimate the amount of power generated by this mechanism of TPG. This methodology is published in source [27]. Sample MATLAB code is given in Appendix B.

2.2.1 System Specification

A simple proof-of-concept device, consisting of a thermoelectric sandwiched between two heat exchangers, was designed with the principles outlined in Chapter 2.1. A mockup of this device is displayed in Figure 3.
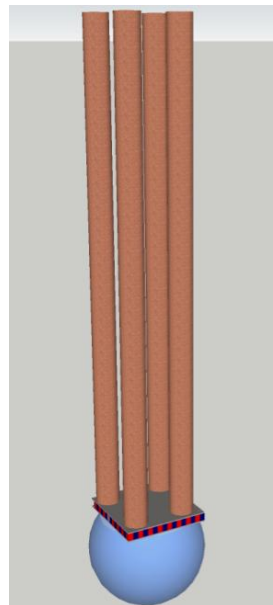
Figure 3:   Proposed proof-of-concept thermoelectric device for dynamic temperature environments.

This device consists of three primary components. The thermoelectric plate is a standard module often sold as a Peltier cooler; it lies below a rapid heat exchanger and above a slow heat exchanger. The rapid heat exchanger was selected as a series of four copper rods mounted to a thin copper film; since copper has a relatively low heat capacity and density and the rod geometry has a high surface-area-to-volume ratio, these material and geometry selections are appropriate for a rapid heat exchanger. A quartz sphere was chosen as the slow heat exchanger; this object has a low surface-area-to-volume ratio and a high heat capacity and density. Again, at this point, the device design emphasizes ease of simulation and experimentation, not the power output, the economic feasibility, or the proposed application. Both heat exchangers have small Biot numbers to initially use a lumped parameter analysis, allowing the numerical simulation to focus on accurately representing the modes of heat transfer.

The physical properties of the heat exchanger materials are tabulated in Table 1.

Table 1: Physical properties of the heat exchanger materials [28–31].

Heat Exchanger	Material	Thermal conductivity, κ (W/m-K)	Specific heat, C_p (J/mol-K)	Density, ρ (g/cm^3)	Absortivity, a	Emissivity, ε
Slow	Quartz	1.4	44.2	2.635	-	-
Rapid	Copper	401	24.6	8.96	0.7	0.78

2.2.2 Numerical Model

With a suitable device design, a heat transfer simulation is developed. This simulation models the device in a desert environment, since the environmental

temperature profiles of these environments are simple and easily created with online weather data. The environmental temperature was assumed to approximate Death Valley, CA, in July to simulate an extreme dynamic temperature environment. The modes of heat transfer present in this system are illustrated in Figure 4.
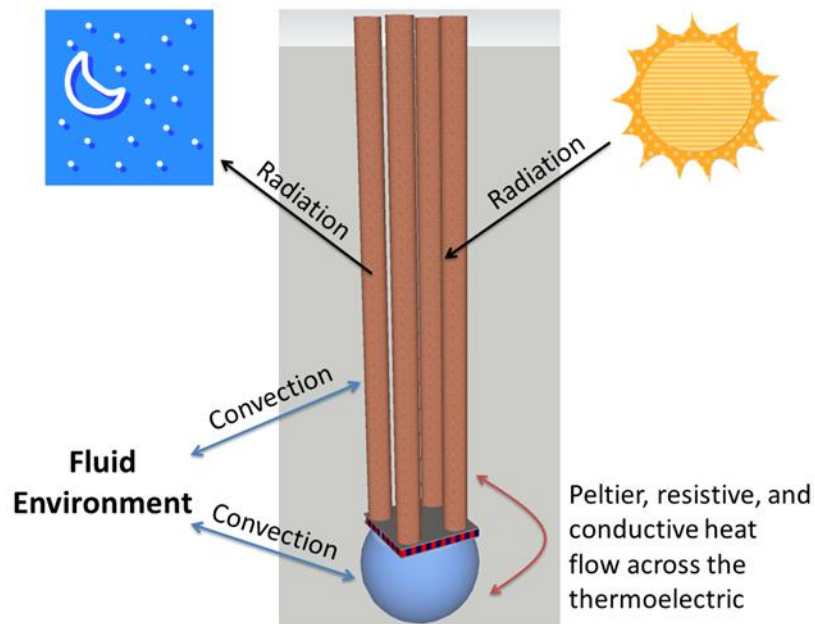
Figure 4:   External and internal modes of heat transfer of the device.

Most of the modes of heat transfer of Figure 4 are well defined; the most difficult part of this analysis is determining the temperature of the heat exchangers. As discussed in Chapter 2.1, various approximations can be made for the spatial and temporal temperature profiles of the heat exchangers, depending on the Biot number. For small heat exchangers (small Biot numbers), the lumped-parameter approximation can be used, vastly simplifying the model development, whereas the temperature

dependence on time for large heat exchangers (large Biot numbers) is often assumed to follow the penetration model.

Using a difference-based, as opposed to a differential-based, model, the temperature of each heat exchanger can be approximated by Equation 6:

$$T(t) = T(t - \Delta t) + \frac{\Sigma \dot{Q}}{MC_p} \Delta t \tag{6}$$

Here, $T(t)$ is the temperature of the heat exchanger as a function of time, $T(t-\Delta t)$ is the temperature of the heat exchanger at the previous time step, $\Sigma \dot{Q}$ is the sum of all modes of heat transfer to the heat exchanger, M is the mass of the heat exchanger, and Δt is the time step. The time step must be less than the characteristic time step τ for both heat exchangers, defined in Equation 7:

$$\tau = \frac{L^2 \rho C_p}{\kappa} \tag{7}$$

The power is thus modeled with Equation 8, a variant of Equation 2:

$$P = \frac{(\alpha(T_{hot} - T_{cold}))^2}{R} \tag{8}$$

where T_{hot} and T_{cold} are the temperatures of the hot and cold heat exchangers, respectively, and R represents the total resistance, or the sum of the internal resistance of the thermoelectric and the external load resistance.

2.2.2.1 Convective Modes

Convective heat transfer between the environment and the heat exchangers is a dominant mode of heat transfer in this system. Newton's law of convection is stated in Equation 9:

$$\dot{Q}_{convective} = hA(T_a - T) \tag{9}$$

The area of heat transfer is taken as half of the sheath area of the rods and the entire surface area of the truncated sphere, based on the correlation requirements.

Although the convective heat transfer coefficient is measured experimentally in the comparison of experimentally-based models to experiment, the original model used empirical correlations, based on Equation 10, to estimate these values.

$$h = \frac{\text{Nu } \kappa_a}{r} \tag{10}$$

In this equation, Nu is the Nusselt number, κ_a is the thermal conductivity of air, and r is the characteristic length of the heat exchangers, taken to be the radius of a rod or sphere. The Nusselt number correlations for the sphere [32] and rod [33] for the applicable conditions are as follows:

$$\text{Nu}_{\text{sphere}} = 2 + 0.6 \, \text{Re}_{\text{sphere}}^{1/2} \, \text{Pr}^{\frac{1}{3}} \tag{11}$$

$$
\begin{aligned}
\text{Nu}_{\text{rod}} = & \left[\left(0.376 \, \text{Re}_{\text{rod}}^{\frac{1}{2}} + 0.057 \, \text{Re}_{\text{rod}}^{\frac{2}{3}} \right) \right. \\
& + 0.92 \left(\log \frac{7.4055}{\text{Re}_{\text{rod}}} \right. \\
& \left. + 4.18 \text{Re}_{\text{rod}} \right)^{-\frac{1}{3}} \left. \text{Re}_{\text{rod}}^{\frac{1}{3}} \right] \text{Pr}^{\frac{1}{3}}
\end{aligned}
\tag{12}
$$

The Prandtl number, Pr, is for ambient air, and the Reynolds number, Re, is defined as follows:

$$\text{Re} = \frac{U_a r}{\nu_a} \tag{13}$$

13

In this equation, U_a and v_a are the velocity and kinematic viscosity of dry air. Relevant physical properties of air are tabulated in Table 2. The velocity of air was assumed to be 0.894 m/s for convenience (i.e. to use the tabulated properties).

The relevant physical properties of dry air are tabulated in Table 2.

Table 2:   Relevant physical properties of dry air [30].

Thermal conductivity, κ (W/m-K)	Prandtl Number, Pr	Kinematic Viscosity, v (m^2/s)	Velocity, U (m/s)
0.03	0.697	2.056 x 10^{-5}	0.894

2.2.2.2   Trans-Thermoelectric Modes

Modes of heat transfer across the thermoelectric include conduction through the thermoelectric elements, conduction through the air between the thermoelectric elements, Peltier heating, Joule heating, and Thomson heating. These modes are generally small relative to convection at these temperatures. For this system, the Thomson effect and conduction through the air between the thermoelectric elements are expected to be small and thus neglected in this model.

2.2.2.2.1   Conduction

Conduction through the thermoelectric elements is modeled by Equation 14:

$$\dot{Q}_{cond} = \frac{\kappa_{TE}\left(fA_{x,TE}\right)}{l_{TE}}\left(T_{rods} - T_{sphere}\right) \tag{14}$$

In Equation 14, (fA_{TE}) and l_{TE} represent the cross-sectional area of the thermoelectrics comprised of thermoelectric elements, as opposed to air, and the thickness of the thermoelectrics, respectively. The f denotes a fill factor, or the fractional area of the thermoelectric plate consisting of thermoelectric elements

14

instead of air. Here, the heat transfer convention was arbitrarily defined as positive for heat flow from the rods to the sphere.

2.2.2.2.2   Peltier Heating

Peltier heating is modeled by Equation 15:

$$\dot{Q}_{Peltier} = N\alpha TI \tag{15}$$

Here, N is the number of elements and I is the current, which is estimated by Equation 16:

$$I = \frac{\alpha\sigma\left(T_{rods} - T_{sphere}\right)(fA_{TE})}{2l} \tag{16}$$

Note that when the rods are warmer than the quartz sphere, the current is positive, resulting in the Peltier effect adding heat to the sphere and removing heat from the rods.

2.2.2.2.3   Resistive (Joule) Heating

Thermal resistance across the thermoelectric also heats the heat exchangers. Here, the resistive heating across the thermoelectric is assumed to go evenly into both heat exchangers. The rate of resistive heating added to each exchanger is given by Equation 17:

$$\dot{Q}_{resistive} = \frac{1}{2}\frac{NI^2 l_{TE}}{(fA_{TE})\sigma} \tag{17}$$

2.2.2.3   Radiative Modes

Radiative heat transfer was considered separately to isolate its effect, allowing the simulation to initially focus on convective heat transfer. Radiation was approached

differently for the numerical model and the models for the experimental simulations. In both cases, radiative heat transfer was only considered for the rods, as a device in a radiative environment would be optimized by only exposing the rapid heat exchanger to radiation.

2.2.2.3.1 Theoretical Radiation Modeling

For the original numerical model, radiation was divided into two phases: radiation from the Sun to the rods during the daytime and radiation from the rods to the night sky. Radiation from the Sun to the rods is given by Equation 18:

$$\dot{Q}_{radiation,rods,day} = a_{rods} A_{rods} q_{rad} \qquad (18)$$

In this equation, a represents absorptivity and q_{rad} represents the solar radiative flux reaching the surface of the Earth. In *Bomberger* [27], q_{rad} was represented by a function fitted to match the summer Sun angles in Death Valley, as in Equation 19:

$$q_{rad} = C_0 + C_1 \sin\left(\frac{\pi(t + C_2)}{C_3}\right) \qquad (19)$$

Here, t is time measured in seconds from 9:00 a.m., and C_0, C_1, C_2, and C_3 are fitting parameters as given in Table 3.

Table 3:   Fitting parameters for radiative exchange between the copper rods and the sun, based on the angle of the sun as a function of time (starting at 9:00 am) in Death Valley, CA, on July 10th, 11th, and 12th, 2011 [32,34]. These parameters are used in Equation 19.

C_0, W/m^2	C_1, W/m^2	C_2, s	C_3
0.0060	1.12537	10,836	43,210

By assuming a constant amplitude, a constant period of 24 hours, and no phase shift, the sinusoidal function in Equation 19 can be easily simplified to Equation 20:

$$q_{rad} = \begin{cases} \beta \sin\left(\dfrac{2\pi}{B}t\right) & \sin\left(\dfrac{2\pi}{B}t\right) \geq 0 \\[2ex] 0 & \sin\left(\dfrac{2\pi}{B}t\right) < 0 \end{cases} \qquad (20)$$

Here, β is the solar constant, commonly accepted as 1360 W/m^2 [35], B is the period of a day (i.e. 24 hours), and t is time measured in seconds from 6 am. The piecewise function simply defines the radiative flux to be zero when the sine function is negative (i.e. during the nighttime). This equation could be similarly constructed for other period lengths.

Assuming the night sky acts as a black body [32], radiation from the copper rods to the night sky is given by Equation 21:

$$\dot{Q}_{radiation,rods,night} = \varepsilon_{rods} A_{rods} \sigma_{SB} \left(T_{night\ sky}^4 - T_{rods}^4 \right) \qquad (21)$$

In this equation, ε represents radiative emissivity and σ_{SB} represents the Stefan-Boltzmann constant. The temperature of the night sky is taken to be 3 K [32]. As energy is exiting the rods, this heat flow will be negative.

2.2.2.3.2 Experimental Radiation Modeling

In experimental simulations, solar radiation was approximated by a halogen bulb with a sinusoidally oscillating power supply in a reflective temperature chamber (as detailed in Chapter 2.3.4). As these conditions differ substantially from the original numerical simulation's conditions, the portion of the numerical model estimating solar radiation was adjusted to reflect this experimental approximation. During the "day", the bulb was assumed to be a point source, with the flux following the inverse square law of intensity (Equation 22):

$$q_{rad} = \frac{P_{bulb}}{4\pi d^2} \qquad (22)$$

Here, P_{bulb} is the power given by the halogen bulb, and d is the distance from the centerpoint of the rod array to the center of the bulb. The power emitted by the bulb is given by Equation 23:

$$P_{bulb} = \begin{cases} P_{bulb,max} \sin\left(\frac{2\pi}{B}t\right) & \sin\left(\frac{2\pi}{B}t\right) \geq 0 \\ 0 & \sin\left(\frac{2\pi}{B}t\right) < 0 \end{cases} \qquad (23)$$

Here, $P_{bulb,max}$ represents the maximum power supplied to the bulb. In this case, the rated power draw of the bulb was taken as this parameter (70 W). The period of the experimental simulations generally was not 24 hours but more often smaller time increments to expedite data collection.

During the "night" (i.e. when the light bulb was off), radiative heat transfer between the rods and night sky was assumed to be nonexistent, as the sky and the rods were very nearly at the same temperature.

2.2.3   Model Assumptions

Assumptions made in this model are listed in this subsection.

2.2.3.1   General Assumptions

- The device environment approximates the conditions of Death Valley in the summer.

- The environment is at a uniform temperature, and heat transfer between the air and the device do not change that temperature.

- A difference-based model with discrete time steps is assumed, as opposed to a computationally intensive differential model. The time step is less than the smaller of the two heat exchanger time steps, justifying this assumption.

- The devices were assumed to be zero-dimensional, meaning their temperature is spatially uniform. This assumption is typically justified by a lumped-parameter analysis, where objects with Biot numbers significantly less than

unity are considered spatially uniform. This assumption is actually only justified for the smallest device, which was specifically chosen to satisfy the lumped parameter analysis. The sphere of the smallest device has a Biot number of 0.29, resulting in a temperature difference between the center of a sphere and the surface of the sphere of about 15% [36]. Although the assumption is not valid for the largest devices due to the size of the quartz sphere, the assumption greatly simplifies computation; that benefit was considered worthwhile, even at the expense of diminished model accuracy. All copper rod assemblages satisfy this approximation.

- Thermal properties, including density, specific heat capacity, thermal conductivity, local heat transfer coefficients, absorptivity, and emissivity, do not change substantially over the given temperature range.

- Measured values were taken for all easily measurable quantities, namely mass, lengths, resistances, Seebeck coefficients, and heat transfer coefficients. Manufacturer's specifications or other sources were used for other properties.

2.2.3.2   Thermoelectric Assumptions

- Using the apparatus and procedure outlined in Dongmo *et al.* [11], "effective" Seebeck coefficients of the entire thermoelectric module were measured and used in the model.

- The temperature gradient seen by the thermoelectric is equal to the temperature difference between the two heat exchangers. This temperature difference is used for calculating power.

- The thermoelectric plate does not store heat.

- The thermoelectric plate is isolated from the environment, meaning no heat transfer occurs between the plate and the environment.

- The energy removed from the system by electricity is negligible relative to the total energy flow.

- The thermoelectric module, comprising the ceramic plates and thermoelectric elements, negligibly contribute to conductive resistance. Two competing considerations arise from this assumption, particularly concerning the ceramic plates. As stated in Bomberger *et al.* [27]:

  "The ceramic plates lie at the interface between the heat exchangers and the thermoelectric module. Thus, at any given instant in time, they

would reduce the temperature differential across the thermoelectric and reduce the output power at that time. However, by introducing additional thermal resistance, the ceramic plates would help to insulate the two heat exchangers from each other and maintain their temperature differential, extending the time period over which power is produced. Thus, neglecting the ceramic plates lead to a slight overestimation of the power output at any given time, but the time period over which power is produced is somewhat conservative. Since the ceramic plates have much higher thermal conductivity compared to the thermoelectric elements, we believe these effects to be relatively small."

In the experimental models, an "effective" Seebeck coefficient is used, eliminating the concerns of overestimated power. Either way, this assumption is not believed to be significant.

- The fill factor of the thermoelectric was calculated by $Nw^2/A_{x,TE}$, where w is the width of the square thermoelectric elements.

2.2.3.3 Quartz Sphere Assumptions

- The quartz sphere is perfectly truncated. The truncation distance was measured for each sphere to the nearest millimeter.

- The sphere of the 22mm device, which was made of soda-lime glass, was assumed to be 95% glass and 5% air, making the density of the glass 95% of that calculated using the measured mass and the volume calculated by the measured radius. The four reconstituted quartz spheres (50mm, 80mm, 110mm, and 130mm devices) were assumed to be 100% quartz.

- The quartz spheres are assumed to be suspended in air, as the effects of the device stand on heat transfer were assumed negligible.

- The quartz sphere was assumed to receive no radiation, as a realistic device would likely be engineered for only one heat exchanger to receive radiation to improve performance.

2.2.3.4 Copper Rod Assumptions

- The effects of the acrylic rod supports on heat transfer were assumed negligible.

- In radiative environments, the rods did not shade other rods. The rods placement was designed to reduce shading.

2.2.3.5 Conductive Heat Transfer

- The thermal resistance of thermal epoxy is negligible relative to other sources of thermal resistance, meaning the thermal conductivity of epoxy is infinite by comparison.

- Joule heating and resistive heating are assumed to distribute the heat equally into each heat exchanger.

- Given the small temperature range, the Thomson effect is negligible.

2.2.3.6 Convective Heat Transfer

- Convective heat transfer does not occur between the thermoelectric plate and the environment.

2.2.3.7 Radiative Heat Transfer (Original Model)

- Sunlight to the rods is evenly distributed.

- At night, the copper rods radiate heat to the sky, which is assumed to be a black body.

- Radiative heat transfer does not occur between the device and Earth.

2.2.3.8 Radiative Heat Transfer (Experimental Model)

- Although the theoretical and experimental models are different for radiation, the amount of radiation received by the device is assumed to be similar in both cases. The experimental solar simulator was designed to emit a similar light intensity (~1000 W/m^2) to that of the Sun. The decision to model the two scenarios separately arises from a desire to both eliminate a mode of heat transfer with high uncertainty and model a scenario that could occur in practice.

- The lightbulb is assumed to be a point source.

- All light eventually reaches the copper rods, as the walls of the temperature chamber are highly reflective, absorbing a negligible amount of light.

- At night, negligible radiation occurs, as the device and its environment are at about the same temperature. The amount of radiation sent from the device to the sky at "night" differs significantly between theory and experiment.

2.3   Experimental Simulations

After the numerical model was built, experimental verification was conducted. This methodology is published in source [37].

2.3.1   Device Construction

Using this theory, we built five devices with varying heat exchanger sizes and configurations, as shown in Figure 1. Consistent with the model [27], a series of 10cm long copper rods attached to a heat-spreading copper foil by thermal epoxy and a truncated quartz sphere were selected as the rapid and slow heat exchangers, respectively. The quartz spheres were professionally truncated (giving a truncated area approximately equal to that of the thermoelectric plate) and smoothed by a glass machinist. The thermoelectric elements were composed of bismuth telluride, the industry standard thermoelectric material for low-temperature (<400 K) TPG applications [15]. The heat exchangers were bonded to the thermoelectric plate using thermally conductive silver epoxy. Acrylic support plates were constructed to secure the vertically upright copper rods; the supports were assumed to have a negligible effect on effective rod surface area and heat transfer coefficient. Thermocouples were epoxied between the lower ceramic plate of the thermoelectric and the quartz sphere, as well as between the upper ceramic thermoelectric plate and the copper foil. The devices were supported by various stands that minimally contact the quartz spheres, as

shown in Figure 5. Device specifications are given in Table 4; for ease of reference, each device is referred to by the diameter of its quartz sphere.
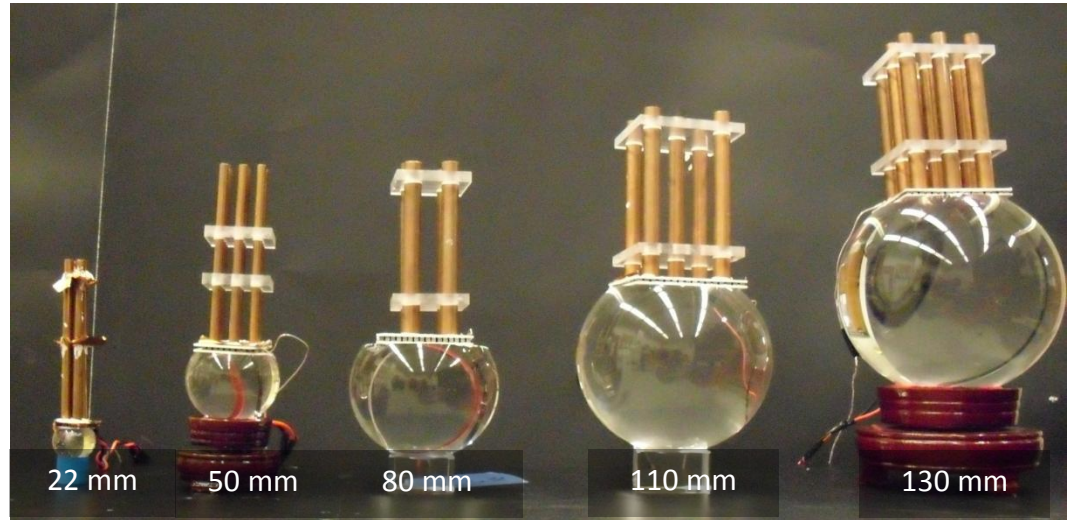
Figure 5:   Device geometries tested (labels indicate sphere diameters).

Table 4:   Specifications of the five devices.

Sphere Diameter (mm)	Sphere Truncation Distance (mm)	Number of Copper Rods	Copper Rod Diameter (mm)	Thermoelectric Area (mm^2)	Number of Thermoelectric Couples
22	4	4	4.76	15x15	31
50	11	9	4.76	36x36	49
80	13	4	9.53	50x50	127
110	15	5	9.53	62x62	127
130	13	9	9.53	62x62	127

2.3.2   Experimental Procedure

Each device was placed in a temperature-controllable chamber (Espec ECT) and connected to an external resistor approximately load-matched to the internal

resistance of the thermoelectrics. After allowing the device to equilibrate at 34°C, the temperature of the chamber was sinusoidally varied from 20°C to 48°C to match the amplitude of a diurnal cycle. The sinusoidal temperature profile of the environment was approximated by about 10-15 discrete steps, as only stepwise set-point temperature changes were accommodated by the temperature controller of the chamber. The voltage across the resistor and the temperatures of the environment and the heat exchangers were logged using a digital multimeter (Keithley 2100) and a thermocouple data acquisition device (Omega TC-08), respectively. Power was calculated for each measurement using $P=\Delta V^2/R$; for comparison, power was also calculated using $P= (\alpha\Delta T)^2/R$, but no results were analyzed from these calculations.

2.3.3 Insulation

Another method of increasing the ratio of heat exchanger thermal response rate coefficients is to insulate the slow heat exchanger. Adding insulation reduces the thermal response rate coefficient of the quartz sphere, largely due to the reduction in its effective heat transfer coefficient. The spheres of the smallest and largest devices were tightly wrapped in thin (3.175mm) polyester insulation. This method of attachment limited the number of layers of insulation that could be conformably added.

2.3.4 Solar Radiation Simulator

The effect of solar radiation on power output was also examined in conjunction with temperature oscillation. To simulate the spectrum of solar radiation, a halogen bulb rated for 70 W was placed inside the temperature chamber 24 cm away from the center of the copper heat exchanger. The quartz spheres of the devices were loosely

wrapped in aluminum foil to limit radiative heat transfer to only one heat exchanger. Using pulse width modulation [38] with a solid-state relay, a LabJack, and a modified version of a stock LabVIEW program, the power to the bulb was sinusoidally varied from zero, to 70 W, and back to zero for half of the period of temperature oscillation and set to zero for the remaining half, approximating the solar cycle.

2.3.5 Modeling the Experimental Devices

Theoretical models were created for the five different devices. Simple device properties, including the heat exchanger masses, thermoelectric Seebeck coefficients, and resistances, were measured experimentally. The only significant deviation from these methods was in estimating the heat transfer coefficients of the heat exchangers experimentally using the procedure given by Russell *et al* [26]. As detailed in Chapter 2.2.2.1, the initial model derived these values from empirical correlations, calculating values ranging from 28.2 W/m^{2}K to 46.4 W/m^{2}K and from 36.3 W/m^{2}K to 133.3 W/m^{2}K for the copper and quartz heat exchangers, respectively. These values overestimate the power output. Literature values for the heat transfer coefficient of heat exchangers with similar geometry and materials could not be found. Instead, the heat transfer coefficients of the heat exchangers were found experimentally by logging the temperature of an isolated heat exchanger as it soaks in the temperature chamber at 50 °C from room temperature and then linearly fitting the data as in Equation 24:

$$\ln\left(\frac{T(t=0) - T_a}{T(t) - T_a}\right) = \left(\frac{hA}{\rho C_p V}\right) t \tag{24}$$

where *t* represents the elapsed time at that measurement. Using this procedure, approximate heat transfer coefficients of 25 W/m^{2}K for a quartz sphere and 20 W/m^{2}K for a copper rod were obtained. These values were not found to vary significantly with

heat exchanger size. With this modification, the model is in excellent agreement with experiment.

Radiative environments were studied separately to obtain results for applications without solar radiation and reduce sources of experimental error.

Chapter 3

RESULTS AND DISCUSSION

3.1   Comparison of Theory and Experiment

By implementing the modifications of Chapter 2.2.5, the model is in reasonable agreement with experiment without requiring the use of a fitting parameter. Experimental and theoretical power profiles for one device size (110mm) are compared in Figure 4 for an environmental oscillation period of 1 hour, illustrating the close match between theory and experiment. As expected, the power profile exhibits a frequency that is double the oscillation frequency of the environmental temperature; the rapid heat exchanger is warmer than the slow heat exchanger during positive excursions of the environmental temperature, resulting in the first power peak, and cooler than the slow heat exchanger during negative excursions, resulting in the second power peak. The device generally takes about three cycles to attain dynamic equilibrium with the environmental temperature profile; therefore, the amplitudes of the first three power peaks of the power profile differ from those of subsequent peaks. The shape of the power profile approximately repeats after the first three peaks.
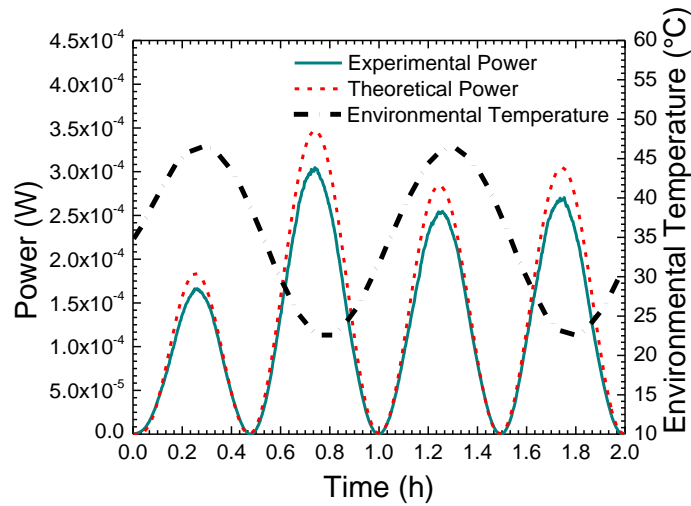
Figure 6:   Experimental and theoretical power profiles for the 110mm device and
             the corresponding environmental temperature profile with an
             environmental sinusoidal temperature oscillation period of 1 hour.

3.2   Optimization

After verifying the model, the focus of this project turned to increasing the

power output of these devices. Sources of optimization studied include the heat

exchanger and the environment.

3.2.1   Heat Exchanger Optimization

Two heat exchanger properties – the size/geometry and the presence of an

insulating coating – were found to have a dramatic effect on the power output.

3.2.1.1   Size and Geometry

The effect of heat exchanger size and geometry on power output was tested

with the five device configurations (Table 4), of which the most significant geometric

variation is the diameter of the quartz sphere. Since all five devices used the same heat

exchanger materials and the value of h is roughly constant, the ratio of heat exchanger thermal response rate coefficients reduces to the ratio of heat exchanger surface area-to-volume ratios (A/V). Furthermore, since A/V of a sphere is inversely proportional to its radius, a larger quartz sphere corresponds to a smaller K_{slow}. Hence, the ratio K_{rapid}/K_{slow} increases for a given K_{rapid}, increasing the power generation. Increasing the device size (mostly by increasing the sphere radius but also the number and size of the copper rods and thermoelectric elements) generally increases the power output, as shown in Figure 3. The power output eventually levels off with increasing device size for $K_{rapid}/K_{slow} > 3.5$.
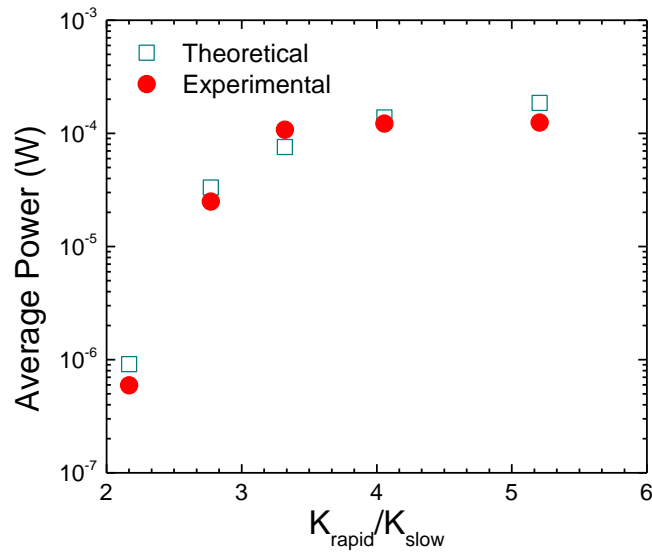
Figure 7:   Experimental and theoretical average TPG as a function of the ratio of thermal response rate coefficients of the heat exchangers for an oscillation period of 1 hour.

29

3.2.1.2 Insulation

Another method of increasing the ratio of heat exchanger thermal response rate coefficients is to insulate the slow heat exchanger. Adding insulation reduces the thermal response rate coefficient of the quartz sphere, largely due to the reduction in its effective heat transfer coefficient. The spheres of the smallest and largest devices were wrapped in thin (3.175mm) polyester insulation, although this method of attachment limited the number of layers of insulation that could be conformably added. The effect of insulation is illustrated by Figure 6 where the theoretical average power is plotted against the quartz heat transfer coefficient for three values of the copper heat transfer coefficient. The average TPG decreases sharply for the particular value of the sphere's heat transfer coefficient at which K_{rapid}/K_{slow} approaches 1. At this point, the rates of temperature change for both heat exchangers are identical, so no power is generated. Figure 7 shows the increase in measured TPG by adding layers of insulation to our smallest device (22mm) for an oscillation period of 1 hour. We observed an increase in average generated power per cycle from $5.9\pm0.8 \times 10^{-7}$ W to $1.9\pm0.1 \times 10^{-6}$ W with one layer of insulation on the quartz sphere and an increase to $7.45\pm0.04 \times 10^{-6}$ W with three layers of insulation for 1 hour periods. With one layer of insulation on the quartz sphere of our largest device (130mm), average TPG increased from 0.124 ± 0.004 mW to 0.160 ± 0.002 mW. Insulation is an effective means of improving device power output without dramatic increases in heat exchanger size.
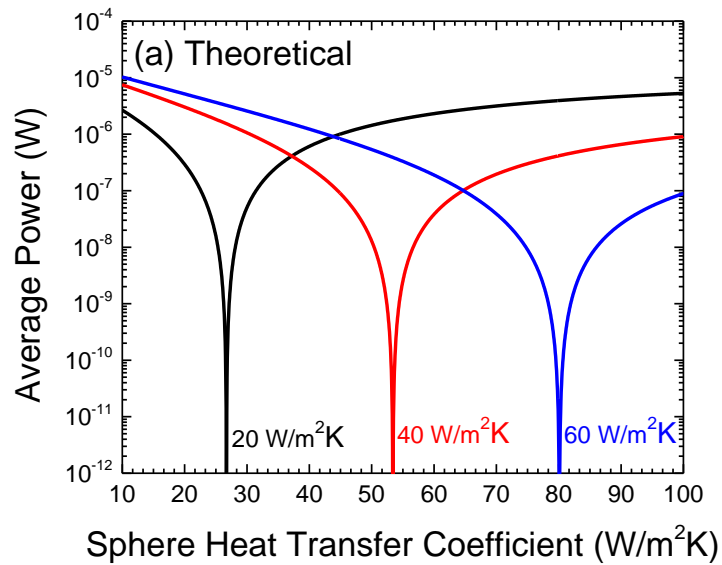
Figure 8:   Simulated average power as a function of heat transfer coefficients for the 22 mm device in an environment with a 1 hour oscillation period. Curves are presented for the copper heat transfer coefficient.
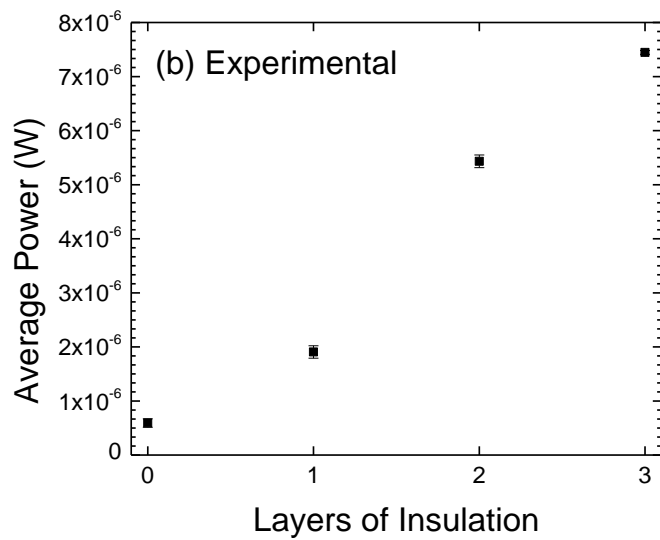
Figure 9:   Experimental average power as a function of the number of layers of insulation on the 22 mm quartz sphere with a 1 hour period of oscillation.

3.2.2   Environmental Effects

In this section, the effects of the period of environmental temperature oscillation (i.e. 24 hours for Earth) and the presence of solar radiation are detailed.

3.2.2.1   Period of Environmental Temperature Oscillation

To test the effect of the environmental temperature oscillation period on TPG, the power was measured for temperature chamber periods of 1, 3, and 5 hours. The period of oscillation of the device's environment was found to be a significant factor in power output, as shown in Figure 8. From theory, all of the devices produce maximum power if the period of oscillation is between 0.5 and 1 hour. For oscillation periods smaller than the optimum, the environmental temperature is fluctuating too quickly for the temperature of the rapid heat exchanger to fully equilibrate, resulting in a small temperature difference across the thermoelectric plate. For oscillation periods larger than the optimum, both heat exchangers have sufficient time to come into thermal equilibrium with the environment, again resulting in a small temperature difference across the thermoelectric plate.
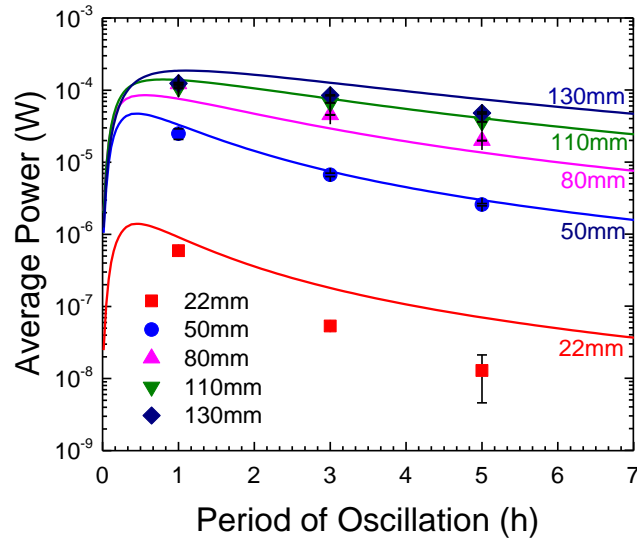
Figure 10: Comparison of theoretical and experimental average TPG for different device geometries and periods of oscillation. Model predictions are represented by solid lines, and the corresponding experimental results are represented by symbols. Note that the experimental points for the largest two devices closely overlap.

3.2.2.2   Solar Radiation

The addition of radiative heat transfer to the copper rods increased TPG by 39%-98%, a range similar to that predicted by the model (45%-98%). The increase in power is due to the partially oxidized copper rods absorbing incident radiation during the positive temperature oscillations and the subsequent increase in the temperature difference across the thermoelectric.
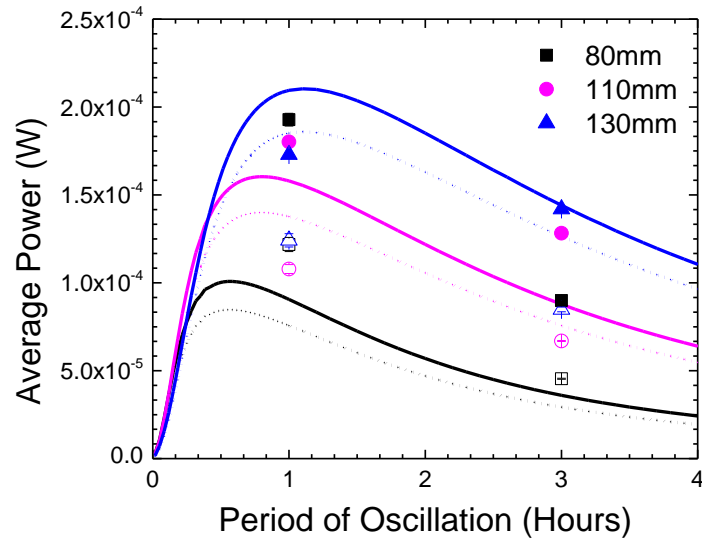
Figure 11: Average power as a function of the period of oscillation for the 80mm, 110mm, and 130mm devices. Lines indicate modeling results, while shapes represent experimental results. Solid lines and filled shapes represent runs with radiation, whereas dashed lines and empty shapes represent runs without radiation.

3.3   Cost Estimations

Assessments of the feasibility of these devices in real-world settings are aided by preliminary cost estimates. The actual materials costs of each device are tabulated in Table 5. The three most significant components of the cost – the two heat exchangers and the thermoelectric – are the only components considered in this analysis. The costs of the acrylic rod supports, epoxy, professional machinists (i.e. to truncate the spheres), and time in the student machine lab were considered negligible or not generally applicable to other devices. Purchases were made in summer 2012.

Table 5: Actual materials cost of the five experimental devices. All costs are rounded to the nearest dollar.

Device's Sphere Diameter (mm)	Thermoelectric Module Cost ($)	Quartz Sphere Cost ($)	Copper Rod Cost ($)	**Total Cost ($)**
22	14	1[a]	14[b]	**29**
50	48	11	31[b]	**90**
80	38	23	34[c]	**95**
110	40	27	42[c]	**109**
130	40	43	76[c]	**159**

[a] These spheres were bought in bulk for $4/lb from a company (Glen Mills) specializing in glass grinding media, so the cost per unit is very small (likely less than $1). Purchasing quartz spheres for similar industrial purposes, instead of from people interested in witchcraft, is a potential source of substantial cost reduction.
[b] These devices used a 3/16" (4.76mm) partitioned copper rod, which cost $0.35/inch.
[c] These devices used a 3/8" (9.53mm) partitioned copper rod, which cost $0.85/inch.

The cost of each of these devices is related to common metrics of power generation in Table 6.

Table 6: Common cost metrics using actual device costs. Maximum and average power values are for an environmental period of 1 hour.

Device's Sphere Diameter (mm)	Raw Material Cost ($)	Cost/Max. Power ($1000/W)	Cost/Average Power ($1000/W)
22	29	11,909	48,968
50	90	1,327	3,612
80	95	287	780
110	109	347	1,011
130	159	470	1,281

Before these devices were tested experimentally, the raw materials for the smallest device (22mm) were estimated at $10 [27]. These devices cost significantly more than initially projected; however, cost was not considered as a design constraint. Moreover, these costs do not incorporate economies of scale, a major source of cost

reductions. For instance, the cost of the heat exchangers is well above the cost of their raw materials, quartz and copper. Quartz, for all intents and purposes, is free. Commodity copper trades at around $3 per pound (as of April 2014); using this value, the cost of the most expensive copper heat exchanger is $0.42. The costs of these devices, assuming the heat exchanger costs are negligible, are tabulated in Table 7.

Table 7:   Common cost metrics assuming the thermoelectric module is the only material cost. Maximum and average power values are for an environmental period of 1 hour.

Device's Sphere Diameter (mm)	Thermoelectric Cost ($)	Cost/Max. Power ($1000/W)	Cost/Average Power ($1000/W)
22	14	5,750	23,600
50	48	708	1,930
80	38	115	312
110	40	127	371
130	40	118	322

Further cost reductions are possible by purchasing the thermoelectrics in bulk. Again, while these devices certainly will not displace industrial or grid-scale electric generators, they could certainly be used to power small sensors or actuators. Such applications are less sensitive to the competitive energy market, as portability and reliability concerns override energy cost.

Chapter 4

CONCLUSIONS AND FUTURE WORK

4.1 Conclusions

In this study, TPG in a dynamic temperature environment has been studied with both theoretical and experimental simulations, and the effects of heat exchanger size, heat exchanger insulation, period of environmental temperature oscillation, and radiative heat transfer have been investigated. The largest average power outputs are on the order of 10^{-4} W, which is comparable to low-power thermoelectric applications for preamplifiers and sensor control systems [39] and radioisotope-powered probes for space exploration [40]. These types of devices are not designed for large-scale power distribution; rather, they are ideal for generating local power for low-power applications.

With optimization, thermoelectric devices can be designed to provide power in other environments with temporal temperature fluctuations. The temperature fluctuations required to drive these devices can be either periodic, as in the temperature oscillations of the day, or sporadic, as in the motion of marine mammals through thermoclines. This mechanism of generating power is applicable for any heat engine, not just thermoelectric devices. For an application requiring constant power, the generated power could be regulated by combining this device with an energy storage system. Some applications of this type of power source include sensors and signals in remote locations such as the desert and tracking large marine wildlife as

they pass through oceanic thermoclines. Additionally, as thermoelectric efficiency continues to increase [13], the range of applications of these devices will expand.

4.2   Future Work

Some paths for future work are proposed in this section.

4.2.1   Device Prototyping

One important path for future work could include designing and prototyping a device for a practical application. One of the most promising applications considered is a device to power whale tags, which are GPS tracking beacons used by marine biologists to monitor migratory patterns. Marine mammals move through oceanic thermoclines, or layers of water at a distinct temperature, to respire at the ocean surface; this motion effectively creates a sporadic temperature gradient. A thermoelectric-heat exchanger device affixed to a whale's tail could eliminate the need to physically find and temporarily immobilize the whale to change the batteries of the signaling device. This somewhat niche application is ideal for this objective because the beacon requires little power, the size constraints are not limiting, and the practicality of such a device is obvious. Other applications include powering small sensors and signals in remote environments and powering drug delivery and health monitoring in the human body, exploiting the transient temperature gradient of blood pumped by the heart. Practical, previously unconsidered difficulties may arise through the design and prototyping processes, potentially yielding critical insights into design constraints. Additionally, although thermoelectric technology is still reaching maturity, many thermoelectric materials are sufficiently advanced for many low-power applications.

4.2.2 Heat Exchanger Material Uniformity

In this work, the heat exchangers were constructed with different materials. By constructing devices with heat exchangers made from the same material, the effect of heat exchanger geometry can be isolated.

In a related line for future work, the heat exchanger materials can also be externally modified by coating or otherwise modifying the surface of the heat exchanger; for example, paint changes the radiative absorptivity, and surface roughening changes the surface-area-to-volume ratio.

4.2.3 Heat Exchanger Geometry Characterization

An important component of the thermal response rate coefficient is the surface-area-to-volume ratio, so both size and geometry play an important role in optimizing the individual heat exchanger performances. For most geometries, the surface-area-to-volume ratio is inversely proportional to size; for example, this ratio simplifies to *3/r* for a sphere. Generally, rapid heat exchangers (large thermal response rate coefficients) should be small with large surface-area-to-volume ratios, and slow heat exchangers (small thermal response rate coefficients) should be large with small surface-area-to-volume ratios. However, the heat exchanger sizes and geometries are also constrained by the application, as large heat exchangers are not practical in many applications. The development of quantitative relationships between the surface-area-to-volume ratio and the power output is critical in designing devices that efficiently balance small device sizes with large power outputs. These relationships may require models redesigned to use finite element analysis.

4.2.4 Thermoelectric Material Characterization

The performance and efficiency of thermoelectric materials is dependent on temperature, so the operating temperature of the application should closely match the optimum temperature of the thermoelectric material. Additionally, conventional thermoelectric characteristic quantities are not entirely applicable to this scenario. The traditional characteristic quantity for applications with spatial temperature gradients, the figure-of-merit, is inversely proportional to the thermal conductivity, meaning thermoelectrics with high thermal conductivities have low efficiency. However, for thermoelectric applications in dynamic temperature environments, a low thermal conductivity may effectively insulate the thermoelectric elements from the heat exchangers, impeding performance when the temperature gradient across the thermoelectric is dynamically changing. A more appropriate characteristic quantity may be developed for thermoelectrics in these applications.

4.2.5 Radiation Studies

A thorough investigation of the effects of radiation on power output is another worthwhile vein of inquiry. As expected, power output increased in the presence of radiation experimentally, but for a 1 hour period of oscillation, the simulated results were the inverse of what was expected (i.e. the 80mm device generated the most power). Additionally, the experimental and simulated results were in poor agreement. Studying these discrepancies and quantifying the effect of radiation on power output would lead to a more accurate understanding of the interactions between these devices and their real-world environments.

REFERENCES

[1]   Meng F, Chen L, Sun F. A numerical model and comparative investigation of a thermoelectric generator with multi-irreversibilities. Energy 2011;36:3513–22.

[2]   Esarte J, Min G, Rowe DM. Modelling heat exchangers for thermoelectric generators. Journal of Power Sources 2001;93:72–6.

[3]   Benson DK, Tracy CE. Design and Fabrication of Thin Film Thermoelectric Generators. Proceedings of the Fourth International Conference on Thermoelectric Energy Conversion, Arlington, TX, USA: 1982, p. 11–4.

[4]   Chen L, Li J, Sun F, Wu C. Performance optimization of a two-stage semiconductor thermoelectric-generator. Applied Energy 2005;82:300–12.

[5]   Chen L, Gong J, Sun F, Wu C. Effect of heat transfer on the performance of thermoelectric generators. International Journal of Thermal Sciences 2002;41:95–9.

[6]   Mayer PM, Ram RJ. Optimization of Heat Sink–Limited Thermoelectric Generators. Nanoscale and Microscale Thermophysical Engineering 2006;10:143–55.

[7]   DiSalvo FJ. Thermoelectric Cooling and Power Generation. Science 1999;285:703–6.

[8]   Harman TC, Walsh MP, Laforge BE, Turner GW. Nanostructured thermoelectric materials. Journal of Electronic Materials 2005;34:L19–L22.

[9]   Rowe DM. Thermoelectrics, an Environmentally-Friendly Source of Electrical Power. Renewable Energy 1999;16:1251–6.

[10]   Hochbaum AI, Chen R, Delgado RD, Liang W, Garnett EC, Najarian M, et al. Enhanced thermoelectric performance of rough silicon nanowires. Nature 2008;451:163–7.

[11]   Dongmo P, Zhong Y, Attia P, Bomberger C, Cheaito R, Ihlefeld JF, et al. Enhanced room temperature electronic and thermoelectric properties of the dilute bismuthide InGaBiAs. Journal of Applied Physics 2012;112:093710.

[12]   Zide JM, Klenov DO, Stemmer S, Gossard a. C, Zeng G, Bowers JE, et al. Thermoelectric power factor in semiconductors with buried epitaxial semimetallic nanoparticles. Applied Physics Letters 2005;87:112102.

[13]   Biswas K, He J, Blum ID, Wu C-I, Hogan TP, Seidman DN, et al. High-performance bulk thermoelectrics with all-scale hierarchical architectures. Nature 2012;489:414–8.

[14]   Yu C, Kim YS, Kim D, Grunlan JC. Thermoelectric behavior of segregated-network polymer nanocomposites. Nano Letters 2008;8:4428–32.

[15]   Rowe DM, Bhandarim CM. Modern Thermoelectrics. Reston, VA, USA: Reston Publishing; 1983.

[16]   Rowe D, Min G. Evaluation of thermoelectric modules for power generation. Journal of Power Sources 1998;73:193–8.

[17]   Riffat S., Ma X. Thermoelectrics: a review of present and potential applications. Applied Thermal Engineering 2003;23:913–35.

[18]   Kyono T, Suzuki RO, Ono K. Conversion of unused heat energy to electricity by means of thermoelectric generation in condenser. IEEE Transactions on Energy Conversion 2003;18:330–4.

[19]   Bell LE. Cooling, heating, generating power, and recovering waste heat with thermoelectric systems. Science 2008;321:1457–61.

[20]   Hsu C-T, Huang G-Y, Chu H-S, Yu B, Yao D-J. Experiments and simulations on low-temperature waste heat harvesting system by thermoelectric power generators. Applied Energy 2011;88:1291–7.

[21]   Yang J, Stabler FR. Automotive Applications of Thermoelectric Materials. Journal of Electronic Materials 2009;38:1245–51.

[22]   Telkes M. Solar Thermoelectric Generators. Journal of Applied Physics 1954;25:765.

[23]   Kraemer D, Poudel B, Feng H-P, Caylor JC, Yu B, Yan X, et al. High-performance flat-panel solar thermoelectric generators with high thermal concentration. Nature Materials 2011;10:532–8.

[24]   Chen J. Thermodynamic analysis of a solar-driven thermoelectric generator. Journal of Applied Physics 1996;79:2717.

[25]   Henderson J. Analysis of a Heat Exchanger - Thermoelectric Generator System. Intersociety Energy Conversion Engineering Conference Vol. 2, Boston, MA, USA: American Chemical Society; 1979, p. 1835–40.

[26]   Russell TWF, Robinson AS, Wagner NJ. Mass and Heat Transfer. 1st ed. New York, NY, USA: Cambridge University Press; 2008.

[27]   Bomberger CC, Attia PM, Prasad AK, Zide JMO. Modeling Passive Power Generation in a Temporally-Varying Temperature Environment via Thermoelectrics. Applied Thermal Engineering 2013;56:152–8.

[28]   The Engineering ToolBox. Thermal Conductivity of Some Common Materials and Gases. Http://www.engineeringtoolbox.com/thermal-conductivity-d_429.html n.d.

[29]   Scherrerand S, Scherrer H. CRC Handbook of Thermoelectrics. In: Rowe DM, editor. CRC Handbook of Thermoelectrics, New York: CRC Press, Inc.; 1995, p. 211–39.

[30]   The Engineering ToolBox. Dry Air Properties. Http://www.engineeringtoolbox.com/dry-air-properties-d_973.html n.d.

[31]   Bird RB, Stewart WE, Lightfoot EN. Transport Phenomena. 2nd ed. New York: John Wile & Sons, Inc.; 1924.

[32]   Gray WA, Muller R. Engineering Calculations in Radiative Heat Transfer. 1st ed. New York: Pergamon Press; 1974.

[33]   Poirier DR, Geiger GH. Transport Phenomena in Materials Processing. Warrendale: The Minerals, Metals & Materials Society; 1994.

[34]   Omar Reis. Nautical Almanac. http://www.tecepe.com.br/scripts/AlmanacPagesISAPI.isa/pages?date=7/10/11 2004.

[35]   Newport. Introduction to Solar Radiation 2014.

[36]   Oziski MN. Basic Heat Transfer. McGraw-Hill; 1977.

[37]   Attia PM, Lewis MR, Bomberger CC, Prasad AK, Zide JMO. Experimental
       studies of thermoelectric power generation in dynamic temperature
       environments. Energy 2013;60:453–6.

[38]   Hirzel T. PWM. Arduino: Learning Foundations n.d.

[39]   Glosch H, Ashauer M, Pfeiffer U, Lang W. A thermoelectric converter for
       energy supply. Sensors and Actuators A: Physical 1999;74:246–50.

[40]   Bass J, Allen D. Milliwatt radioisotope power supply for space applications.
       Eighteenth International Conference on Thermoelectrics, Baltimore, MD, USA:
       1999, p. 521–4.

Appendix A

NOMENCLATURE TABLE

A Surface area (m^2)

A_x Cross-sectional area (m^2)

a Absorptivity

B Sinusoidal period (s)

C Generic constant

C_p Constant-pressure specific heat capacity ($kJ\ kg^{-1}\ K^{-1}$)

d Distance (m)

f Fill factor

h Heat transfer coefficient ($W\ m^{-2}\ K^{-1}$)

I Current (A)

K Thermal response rate coefficient (s^{-1})

L Empirical characteristic length; often defined as the surface area-to-volume ratio for objects of irregular shape (m)

l Length of thermoelectric elements, i.e. thickness of thermoelectric plate (m)

M Mass (kg)

N Number of thermoelectric elements

P Power (W)

Q Rate of heat flow (W)

q Rate of heat flux ($W\ m^{-2}$)

R Total resistance (Ω)

r Radius of a sphere/cylinder; generally, a correlative characteristic length (m)

ΔT Temperature difference (K)

T Absolute temperature (K)

Δt Time step (s)

t Time, relative to reference time (s)

U Velocity ($m\ s^{-1}$)

ΔV Voltage (V)

V Volume (m^3)

w Width of a thermoelectric element (m)

Z When multiplied by T, dimensionless thermoelectric figure-of-merit

Greek symbols

α	Seebeck coefficient (V K^{-1})
β	Solar constant (W m^{-2})
ε	Emissivity
κ	Thermal conductivity (W m^{-1} K^{-1})
ν	Kinematic viscosity (m^2 s^{-1})
ρ	Density (kg m^{-3})
σ	Electrical conductivity (Ω^{-1} m^{-1})
σ_{SB}	Stefan-Boltzmann constant (W m^{-2} K^{-4})
τ	Characteristic time step

Dimensionless numbers (transfer phenomena)

Bi	Biot number
Nu	Nusselt number
Pr	Prandtl number
Re	Reynolds number

Subscripts

a	Generally, ambient environment; specifically in this study, air
rad	Radiation
TE	Thermoelectric

Appendix B

MATLAB CODE

Four MATLAB routines are attached in this appendix:

1. **D110mm.m:** This script initializes the heat exchanger and thermoelectric parameters that are specific to the 110mm device. Each device has its own script that accomplishes the same task.

2. **Constants.m:** This script initializes constants that apply to all five devices, including runtime and thermoelectric constants.

3. **CalculationsAndFigures.m:** This script runs the main heat transfer simulation and then generates useful calculations and figures.

4. **sampler.m:** This function "samples" the larger data array for a given interval and creates a smaller, more manageable array for graphing and analysis

5. **autoanalyze.m:** This script analyzes experimental temperature and voltage data prearranged in an Excel spreadsheet and generates useful parameters, such as the experimental Seebeck coefficient and power statistics

B.1 D110mm.m

```
clear, close all

% Run constants
period = 1;

%Radiation Constants
P = 70; %Power going to the lightbulb [W]

Constants;

% Bottom Object Constants (Based on quartz glass)
% http://www.quartz.com/gedata.html#table
sphereradius = 110 / 2 / 1000; % (inches -> m)
capheight = 15 / 1000; %height of spherical cap (mm -> m)
solidfactor = 1; % Fraction of sphere that is actually soda lime
glass
                       % (as opposed to air bubbles)
spheredensity = solidfactor * 2.2 * 1000; % Sphere density [kg/m^3]
spherevolume = 4/3*pi*sphereradius^3 - ...
    (1/3)*pi*(capheight^2)*(3*sphereradius-capheight); % Sphere
volume (m^3)
spheremass = spheredensity * spherevolume; % Sphere mass [kg]
Afb = 4*pi*sphereradius^2 - 2*pi*sphereradius*(sphereradius -
capheight); % Surface area between bottom object and the fluid
spherekappa = 1.4; %The thermal conductivity of the bottom object
[W/(m K)]
spherecp = 670; % [=] J/(kg * K)
Absb = 0.05;% Absorptance of fused quartz
(http://www.sciner.com/Opticsland/FS.htm#Optical Grade Fused Quartz
(KV))
Re = Vel * sphereradius / nu; %Calculates the Reynolds number for the
bottom object
% Calculates Nusselt number for forced flow past a single sphere for:
    % Reynolds number between 1 and 70000
    % Prandtl number between 0.6 and 400.
% Fluid properties should be based on T@surface + T@infinity / 2
Nu = 2 + 0.60 * Re^0.5 * Pr^(1/3) ;
Hb = Nu * Ka / sphereradius; % heat transfer coefficient [W/(m^2 K)].
Hb = 20;

% Top Object Constants (copper)
n = 5; % Number of rods
rodradius = (3/8) / 2 * 2.54 / 100; % 5 gauge copper wire
rodheight = 100/1000; % Height of the copper rods [mm->m]
roddensity = 8.96 * 1000; % The density of the top object [kg/m^3]
rodvolume = n*(pi*rodradius^2*rodheight); % volume of rods
%rodmass = roddensity * rodvolume; % the mass of the top object [kg]
rodmass = n*62.6533/1000; % measured rod mass [kg]
```

```matlab
Aft = n*pi*rodradius*rodheight; % Area between the rods and the fluid
(1/2 the sheath SA)
rodcp = 385; % [J/(kg * K)]
Kt = 401 ; % Thermal conductivity of top object [W/(m K)]
Re = Vel * rodradius / nu; %Calculates the Reynolds number for one
cylinder
%Correlation basted on the limit that Pr goes to infinity and small
Re
Nu = (0.376*Re^0.5 + 0.057*Re^(2/3))*Pr^(1/3) + ...
     0.92*(log(7.4055/Re) + 4.18*Re)^(-1/3)*Re^(1/3)*Pr^(1/3);
Ht = Nu * Ka / rodradius; % heat transfer coefficient [W/m^2-K].
Ht = 25;
Abst = 0.5; %Dull Cu solar absorptivity
(http://www.solarmirror.com/fom/fom-serve/cache/43.html)


%Thermoelectric Constants
% from http://www.customthermoelectric.com/MaterialProperties.htm
N = 254 ; % The number of elements
Le = 5.1 / 1000; % Length of the elements [mm -> m]
SA = (62/1000).^2; % Surface area of the module, or size of the
ceramic plate (mm -> m)
width = 2.57/1000; % width of the elements [mm->m]
Fillfactor =  N*((width)^2)/SA; % The percentage of the cross-
sectional area of the entire
                  % thermoelectric that is the elements
Atb = Fillfactor * SA; % Contact area between the bottom object and
the TE.
                  % This assumes that the tops of the elements
are
                  % exposed to the air
TEresistance = 1.9; % Internal resistance of thermoelectric
Loadresistance = 1.57;
% Seebeck = 201e-6; % Seebeck coefficent of Bi2Te3 [V/K]
% alpha = N * Seebeck; % Seebeck coefficient of the device [V/K]
alpha = 0.01751526; % Measured Seebeck of the device
(alpha_effective)
Ke = 1.5; % Thermal conductivity of the elements [W/m K]


CalculationsAndFigures
```

B.2 Constants.m

```
% This code initializes the common constants for the General Models
% ('D22mm.m', 'D50mm.m', etc)

disp ('----------------New Run--------------------------')

% Run Constants
runtime = 86400/(24/(2*period)); %in seconds. 86400 seconds equals
one day
dt = 1; % Time step in seconds. dt can be fairly high in this case
samplingrate = 30; % [s]. Try to make this a multiple of dt
freq = (24/period)*(1.1574*10^-5); %Frequency of the fluctuation in
the fluid temp (1 day = 1.1574e-5)[1/s]
amp = 12; % amplitude of the fluid fluctuation in fluid temp [K] (14
is for the desert, july 10 2011)
Tstart = 307; % [=] K: Starting temperature of the device (9am start)

% Fluid constants (dry air)
Ka = 0.03003; % Thermal conductivity of the air [W/(m K)]
Pr = 0.697; % Prandalt number for the fluid
Vel = 1; % Velocity of fluid relative to device [m/s]
nu = 2.056*10^-5; % kinematic viscosity of the fluid [m^2/s]
```

B.3 CalculationsandFigures.m

```matlab
% This code handles all of the calculations for the General Models
% ('D22mm.m', 'D50mm.m', etc)

%Radiation Stuff
rad = 0.25; %distance from the lightbulb (assuming it to be a point
source) to the device
Qradt = Abst*(P/(4*pi*(rad^2)))*(2*Aft); %Radiation to rods from
light bulb, Irradiance*area that is illuminated [J/s], [W]
%Qradb = Absb*(P/(4*pi*(rad^2)))*(Afb); %Radiation to Sphere from
light bulb [J/s]
% Areas are NOT divided by two because it is assumed that all the
radiation eventually reaches the device (due to reflection off the
wall, foil, etc). The Aft is multiplied by 2 because it is 1/2 the
sheath area

%Preallocate Arrays
imax = runtime/dt; %max number of steps to calculate is total run
time/time steps
Tb = zeros(imax, 1); Tt = zeros(imax, 1); Power = zeros(imax, 1);
Qconvsphere = zeros(imax, 1); Qconvrod = zeros(imax, 1);
Qcond = zeros(imax, 1); Qpeltiert = zeros(imax, 1); Qpeltierb =
zeros(imax, 1);
Qresistive = zeros(imax, 1); Qtb = zeros(imax, 1);
I = zeros(imax, 1); V = zeros(imax, 1);

%Sets initial parameters
Time = (0:dt:runtime)'; maxindex = length(Time)-1;
Tf = Tstart + amp * sin(2 * pi * freq .* Time);
Tb(1) = Tstart; Tt(1) = Tstart;
%Radiation
Intensity = sin(2 * pi * freq .* Time);
Intensity(Intensity<0) = 0;

% Calculates heat transfer. Just convection, conduction
% Positive heat flow is taken to be heat transfer into the device
% (more specifically, into the sphere)
for i = 1:maxindex
    Qconvsphere(i) = Hb*Afb*(Tf(i) - Tb(i)); % Fluid-sphere
convection
    Qconvrod(i) = Ht*Aft*(Tf(i) - Tt(i)); % Fluid-rod convection
    Qcond(i) = Ke*Atb*(Tt(i) - Tb(i))/Le; % Rod-sphere conduction

    % Temperature difference to power
    V(i) = alpha * (Tt(i) - Tb(i));
    Power(i) = V(i).^2 / (Loadresistance + TEresistance);
    I(i) = V(i) / (Loadresistance + TEresistance); %Changed from I =
P/V

    Qpeltierb(i) = alpha*Tb(i)*I(i);
```

```matlab
    Qpeltiert(i) = -alpha*Tt(i)*I(i);

    Qresistive(i) = I(i)^2 * TEresistance / 2; % Q = I^2*R

    %Update temperature and convert temp diff to power
    Tb(i+1)= (Qconvsphere(i)+Qresistive(i)+Qpeltierb(i)+Qcond(i))/
...
        (spheremass * spherecp)*dt + Tb(i);
    Tt(i+1)=
(Qconvrod(i)+Qradt*Intensity(i)+Qresistive(i)+Qpeltiert(i)-Qcond(i))/
...
        (rodmass * rodcp)*dt + Tt(i);
end

% Calculates and displays run information and samples the data every
30s
% Time = Time(1:maxindex); Tf = Tf(1:maxindex); Tb = Tb(1:maxindex);
Tt = Tt(1:maxindex);
Time = sampler(Time(1:maxindex),dt,samplingrate); Tf =
sampler(Tf(1:maxindex),dt,samplingrate);
Tb = sampler(Tb(1:maxindex),dt,samplingrate); Tt =
sampler(Tt(1:maxindex),dt,samplingrate);
Power = sampler(Power, dt, samplingrate); V =
sampler(V,dt,samplingrate);
Qconvsphere = sampler(Qconvsphere,dt,samplingrate); Qconvrod =
sampler(Qconvrod,dt,samplingrate);
Qcond = sampler(Qcond,dt,samplingrate); Qpeltierb =
sampler(Qpeltierb,dt,samplingrate);
Qpeltiert = sampler(Qpeltiert,dt,samplingrate);
Qresistive = sampler(Qresistive,dt,samplingrate); Qtb =
sampler(Qtb,dt,samplingrate);
Time = Time/3600/24; %converts to days
deltaT = Tt - Tb;

subplot(2,2,1)
plot(Time, Tf - 273.15, Time, Tt - 273.15, Time, Tb - 273.15)
%legend('T_e_n_v_i_r_o_n_m_e_n_t','T_c_o_p_p_e_r','T_s_p_h_e_r_e')
xlabel('Time (hours)'), ylabel('Temperature (deg C)')

subplot(2,2,2)
plot(Time, Power)
xlabel('Time (days)'), ylabel('Power (W)')

subplot(2,2,3)
plot(Time, abs(deltaT))
xlabel('Time (days)'), ylabel('Temperature Difference (K)')

subplot(2,2,4)
plot(Time, V)
xlabel('Time (hours)'), ylabel('Voltage (V)')
```

```matlab
AveragePower = mean(Power);
fprintf('\nAverage Power = %d W\n', AveragePower)
AveragePowerPerArea = AveragePower / SA ;
%{
fprintf('\nAverage Power per Unit Area = %d W/m^2',
AveragePowerPerArea)
MaxPower = max(Power);
fprintf('\nMaximum Power = %d W', MaxPower)
MaxPowerPerArea = MaxPower / SA;
fprintf('\nMax Power per Unit Area = %d W/m^2', MaxPowerPerArea);
MaxDeltaT = max(deltaT);
fprintf('\nMax DeltaT = %d K', MaxDeltaT);
AverageEnergyPerDay = runtime * AveragePower / 3600;
fprintf('\nAverage Energy per Day = %d W-h/day', AverageEnergyPerDay)
AverageVoltage = mean(abs(V));
fprintf('\nAverage Voltage = %d V', AverageVoltage)
AverageDeltaT = mean(abs(deltaT));
fprintf('\nAverage Temperature Difference = %d K\n', AverageDeltaT)
%}
```

B.4 sampler.m

```matlab
function [ shortenedarray ] = sampler( array, dt, samplingrate )
%SAMPLER takes in an array with a small time step (dt) and returns a
%shorter array with a larger time step
%   INPUTS:
%   -array: original array to be shortened
%   -dt: time step of the input array (s)
%   -samplingrate: time step of new array (s)
%       -e.g.:30 seconds for most applications
%   OUTPUTS:
%   -shortenedarray: new array with larger time step

oldArrayLength = length(array);
totalTime = oldArrayLength * dt;
newArrayLength = totalTime / samplingrate;

shortenedarray = zeros(newArrayLength, 1);

for i=1:oldArrayLength
    if mod(i*dt, samplingrate) == 0
        shortenedarray(i*dt/samplingrate) = array(i);
    end
end


end
```

B.5 autoanalyze.m

```matlab
% Arrange the data in the Excel document as follows:
%   Time, Env 1, Env 2, Env 3, Copper, Sphere, Voltage
% The sheet name should be 'Sheet1'.
clear, close all

fprintf('--------------------New AutoAnalysis--------------------
--\n')

% CHANGE THE INFORMATION BELOW
%%%%%%%%%%%%%%%%%%%%%%%%%%%%%%%%%%%%%%%%%%%%%%%%%%%%%%%%%%%%%%%%%%%%%
%%%%%
% For fileName, enter the full path of the file (NOT including
.xlsx).
% Additionally, delete all excess temperature data from the bottom of
the Excel file
runNumber = 128; % i.e. 58
resistance = 1.57; % load resistance
% If the Seebeck plot doesn't spit out a fitted curve (ie red line),
change thereIsAZero.
% Try false first and then true.
thereIsAZero = false;
%%%%%%%%%%%%%%%%%%%%%%%%%%%%%%%%%%%%%%%%%%%%%%%%%%%%%%%%%%%%%%%%%%%%%
%%%%%

%{
% Manual input, makes things a little slower
date = input('Enter the run date (MM/DD/YY), enclose in single
quotes: ');
period = input('Enter the period length: ');
size = input('Enter the device size: ');
foil = input('Enter either ''Foil'' or ''No Foil'' (with single
quotes): ');
rad = input('Enter either ''Lightbulb'' or ''No Lightbulb'' (with
single quotes): ');
%}

fileName = ['C:\Documents and Settings\Pete\My Documents\Dropbox\TE
experiment\Data\Run ', int2str(runNumber)];
ndata = xlsread([fileName,'.xlsx'], 'Sheet1');

% Makes a plot for the user to select temperatures for thermocouple
% calibration
ndata(:,1) = ndata(:,1) / 3600; % [s] -> [hr]
plot(ndata(:,1), ndata(:,2),ndata(:,1), ndata(:,3),ndata(:,1),
ndata(:,4),ndata(:,1), ndata(:,5),ndata(:,1), ndata(:,6))
xlabel('Time (hours)'), ylabel('Temperature (\circC)')
legend('Env1','Env2','Env3','Copper','Sphere')
start = input('Enter the start time of the steady-state range (in
hours): ');
```

```matlab
stop = input('Enter the end time of the steady-state range (in
hours): ');
size = input('Enter the sphere diameter(in mm): ');

% Returns the indeces of start/stop
[start, ~] = find(ndata==start);
[stop, ~] = find(ndata==stop);

% temps stores all temperature data in the selected range
temps = ndata(start:stop, 2:6);
envAverage = mean2(temps(:,1:2));
copperAverage = mean(temps(:,4));
sphereAverage = mean(temps(:,5));
copperOffset = envAverage - copperAverage;
sphereOffset = envAverage - sphereAverage;

% Adjusts the copper and sphere temperatures by the offset
ndata(:,5) = ndata(:,5) + copperOffset;
ndata(:,6) = ndata(:,6) + sphereOffset;

% Trims the data to only be the 'real' region
start = input('Enter the start time of the cycle (in hours): ');
stop = input(['Enter the end time of the cycle (in hours).\n', ...
    'The end time should be the start time plus twice the period
length: ']);
starthours = start;
stophours = stop;
% Returns the indeces of start/stop
[start, ~] = find(ndata==start);
[stop, ~] = find(ndata==stop);
ndata = ndata(start:stop,:);

close all
% Analysis

% deltaT = sphere - copper
deltaT = ndata(:,6) - ndata(:,5);

% Power (Voltage) = V^2/R
voltages = ndata(:,7);
power = voltages.^2/resistance;
averagePower = mean(power);
maxPower = max(power);

% Seebeck (from SeebeckCalculator.m)
interestingValues = zeros(length(voltages), 3);
index = 1;

for i=1:length(deltaT)
    if contains(interestingValues, deltaT(i))==false
        interestingValues(index, 1) = deltaT(i);
```

```matlab
        index = index + 1;
    end
end

if (thereIsAZero == false)
    index = index -1;
end
interestingValues = interestingValues(1:index,:);
interestingValues = sort(interestingValues,1);


for i=1:length(interestingValues)
    currTempDiff = interestingValues(i,1);
    currentTempDifferenceValues = [];
    for j=1:length(deltaT)
        if (deltaT(j)==currTempDiff)
            currentTempDifferenceValues =
[currentTempDifferenceValues;voltages(j)];
        end
    end
    interestingValues(i,2) = mean(currentTempDifferenceValues);
    interestingValues(i,3) = std(currentTempDifferenceValues);
end


figure
hold on
grid on
errorbar(interestingValues(:,1),interestingValues(:,2),interestingVal
ues(:,3))
xlabel('Temperature'), ylabel('Voltage')
P = polyfit(interestingValues(:,1),interestingValues(:,2),1);
yfit = P(1)*[deltaT voltages]+P(2);
plot([deltaT voltages],yfit,'r-.');
seebeck = P(1);
seebeckError = mean(interestingValues(:,3));
% End seebeckcalculator

% Power (Voltage) = V^2/R
powerSeebeck = seebeck.^2*deltaT.^2/resistance;
averagePowerSeebeck = mean(powerSeebeck);
maxPowerSeebeck = max(powerSeebeck);


disp(averagePower)

% Craete text file
runNumberString = ['Run ',int2str(runNumber)];
mkdir('C:\Documents and Settings\Pete\My Documents\Dropbox\TE
experiment\Data\Analyzed Data\Radiation', runNumberString);
fileID=fopen(['C:\Documents and Settings\Pete\My Documents\Dropbox\TE
experiment\Data\Analyzed Data\Radiation\Run ',
int2str(runNumber),'\Run ', int2str(runNumber),' Results.txt'],'wt');
fprintf(fileID,'Updated %s\n\n',datestr(now,2));
```

```matlab
fprintf(fileID,'Run %d\n',runNumber);
%{
% Outputting the manual info input
fprintf(fileID,'%s\n',date);
fprintf(fileID,'%.2f Ohm Resistor\n',resistance);
fprintf(fileID,'%d hour period\n',period);
fprintf(fileID,'Full %dmm device\n',size);
fprintf(fileID,'%s\n', foil);
fprintf(fileID,'%s\n\n', rad);
%}
fprintf(fileID,'%.2f Ohm Resistor\n', resistance);
fprintf(fileID,'%.2f hour period\n', (stophours-starthours)/2);
fprintf(fileID,'Full %dmm device\n', size);
fprintf(fileID,'Radiation\n\n');

fprintf(fileID,'Unweighted Seebeck = %f +/-
%f\n',seebeck,seebeckError);
fprintf(fileID,'Average Power (Voltage) = %e\n', averagePower);
fprintf(fileID,'Average Power (Seebeck) = %e\n',
averagePowerSeebeck);
fprintf(fileID,'Max Power (Voltage) = %e\n', maxPower);
fprintf(fileID,'Max Power (Seebeck) = %e\n', maxPowerSeebeck);
fprintf(fileID,'Max temperature difference = %f', max(deltaT));
```